

A high-frequency warm shallow water acoustic communications channel model and measurements

Mandar Chitre^{a)}

Acoustic Research Laboratory, National University of Singapore, 12A Kent Ridge Road, Singapore 119223

(Received 30 April 2007; revised 8 August 2007; accepted 9 August 2007)

Underwater acoustic communication is a core enabling technology with applications in ocean monitoring using remote sensors and autonomous underwater vehicles. One of the more challenging underwater acoustic communication channels is the medium-range very shallow warm-water channel, common in tropical coastal regions. This channel exhibits two key features—extensive time-varying multipath and high levels of non-Gaussian ambient noise due to snapping shrimp—both of which limit the performance of traditional communication techniques. A good understanding of the communications channel is key to the design of communication systems. It aids in the development of signal processing techniques as well as in the testing of the techniques via simulation. In this article, a physics-based channel model for the very shallow warm-water acoustic channel at high frequencies is developed, which are of interest to medium-range communication system developers. The model is based on ray acoustics and includes time-varying statistical effects as well as non-Gaussian ambient noise statistics observed during channel studies. The model is calibrated and its accuracy validated using measurements made at sea.

© 2007 Acoustical Society of America. [DOI: 10.1121/1.2782884]

PACS number(s): 43.30.Zk, 43.30.Cq [EJS]

Pages: 2580–2586

I. INTRODUCTION

The ability to communicate effectively underwater has numerous applications for marine researchers, oceanographers, marine commercial operators, off-shore oil industry, and defense organizations. As electromagnetic waves cannot propagate over long distances in seawater, underwater acoustic communication is the core enabling technology for such applications. Underwater acoustic communications has been a difficult problem due to unique channel characteristics such as fading, extended multipath, and refractive properties of the sound channel (Stojanovic, 1996). Attempts at adapting communication techniques developed for other channels have yielded successful implementations in vertical deep water channels, but have had limited success in shallow water channels (Stojanovic, 1996). Although considerable progress has been made in shallow water communication over the past decade, the medium range channel of very shallow warm water, common in tropical coastal regions such as Singapore waters, still poses a challenge to most communication modems (Chitre, 2006). This warm shallow water acoustic (WSWA) channel presents two key features—extensive time-varying multipath (Chitre *et al.*, 2004) and high levels of non-Gaussian ambient noise due to snapping shrimp (Potter *et al.*, 1997a, b; Chitre *et al.*, 2004)—both of which limit the performance of traditional communication techniques. A good understanding of the communications channel is important in the design of a communication system. It aids in the development of signal processing techniques as well as in the testing of the techniques via simulation. In this article, we present a channel model for the WSWA channel and validate it with field experiments.

Ray theory and the theory of normal modes have provided the basis for channel modeling (Coates, 1989). At high frequencies, ray tracing is an appropriate model and is commonly used to determine the coarse multipath structure of the channel. The surface movement and environmental changes can contribute significantly to the variability of a channel. This variability has been modeled and measured (Owen *et al.*, 1994; Badiey *et al.*, 2000). A simpler stochastic channel model has also been developed (Galvin and Coates, 1994). The model has been validated against experimental results from a very shallow water channel in Southampton, UK. In wireless communications, it is common to model a multipath channel using a tapped delay line with tap gains as stochastic processes (Proakis, 1995). When the tap gains are modeled using complex Gaussian processes, the resulting channel is the well-known Rayleigh fading channel. Some researchers consider the shallow water medium range channel to exhibit Rayleigh fading (Catipovic, 1990). Experimental support for such claims is found (Galvin and Coates, 1994). However, the model has been challenged by others (Essebar *et al.*, 1994; Geng and Zielinski, 1995). A hybrid model where the multipath tap delays are computed using a ray model and the tap variation is modeled using Ricean statistics is proposed (Geng and Zielinski, 1995). The motivation for such a channel model is discussed in depth but no results or validation is presented. Although the model is physics based, the model does not include known acoustic propagation physics such as spreading, absorption, etc. Based on a review of literature, currently there seems to be no consensus among researchers as to which channel model is best suited for very shallow water medium range channels.

In warm shallow waters, the ambient noise beyond about 2 kHz is commonly dominated by snapping shrimp (Potter *et al.*, 1997a, b). Snapping shrimp are impulsive sources and

^{a)}Electronic mail: mandar@arl.nus.edu.sg

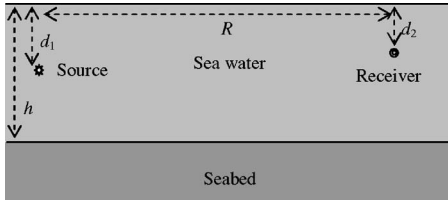


FIG. 1. Schematic showing a Pekeris waveguide model of the WSWA channel.

the pressure amplitude distribution is known to be described well by the symmetric α -stable ($S\alpha S$) distribution (Chitre *et al.*, 2004). The noise amplitude distribution (pressure amplitude in case of acoustics) plays an important role in the analysis of communication schemes. A linear communication receiver designed with a Gaussian noise assumption is sub-optimal in the presence of non-Gaussian noise. Armed with the knowledge of the noise distribution, optimal or near-optimal nonlinear receivers (Tsihrintzis and Nikias, 1995; Chitre *et al.*, 2006) and decoders (Chitre *et al.*, 2007) can be designed for improved communication performance.

In this article, we develop a physics-based channel model for the WSWA channel. The model is based on ray propagation in a well-mixed channel of constant depth. We model each ray to independently fade as described by the Rayleigh distribution. The arrival time of each ray is modeled to statistically vary over time. An additive $S\alpha S$ noise model is adopted to describe the ambient noise. The resulting channel model is calibrated and its accuracy validated using measurements made in Singapore waters.

II. CHANNEL MODEL

In this section, we develop a mathematical model for signal propagation through the WSWA channel. The model is primarily based on the physics of ocean acoustics. In addition, the model includes some statistical variations that are not included in the physics models that we have incorporated.

A. Physics of high frequency underwater acoustic propagation

Acoustic propagation in the ocean is governed by the wave equation. As solutions to the wave equation are difficult to find in general cases, approximations are often used to model propagation. The ray theory provides one such approximation, commonly used for high frequency propagation modeling (Brekhovskikh and Lysanov, 1991). As medium range communication signals are usually high frequency, we use the ray model as a basis for our model of channel propagation. In the ray model, sound energy is conceptualized as propagating along *rays*, which are straight lines in the case of a fluid medium with a constant sound speed (isovelocity). The rays are partially reflected and partially refracted when they encounter a discontinuity in sound speed. We model the WSWA channel as a Pekeris waveguide, consisting of an isovelocity layer over an isovelocity half-space (Fig. 1). The isovelocity layer models the seawater while the isovelocity half-space models the seabed. The isovelocity assumption for

seawater is justified as WSWA channels are usually well mixed and have relatively small increase in pressure over the depth of the water column. The assumption is further supported by numerous sound speed measurements in Singapore waters (Chitre, 2006). The sea surface is modeled as a pressure-release boundary.

Let d_1 be the depth of the source, d_2 be the depth of the receiver, h be the height of the water column, and R be the transmission range. The distance traveled by the sound along various eigenrays can be computed using the method of images (Brekhovskikh and Lysanov, 1991). The distance along the direct eigenray is denoted by D_{00} given by

$$D_{00} = \sqrt{R^2 + (d_1 - d_2)^2}. \quad (1)$$

Let D_{sb} be the distance along an upward originating eigenray with s surface reflections and b bottom reflections. For such eigenrays, $0 \leq s - b \leq 1$ and

$$D_{sb} = \sqrt{R^2 + [2bh + d_1 - (-1)^{s-b}d_2]^2}. \quad (2)$$

Let \underline{D}_{sb} be the distance along a downward originating eigenray with s surface reflections and b bottom reflections. For such eigenrays, $0 \leq b - s \leq 1$ and

$$\underline{D}_{sb} = \sqrt{R^2 + [2bh - d_1 + (-1)^{b-s}d_2]^2}. \quad (3)$$

We assume that our source is omnidirectional and therefore produces a spherical wavefront in an isovelocity medium. The energy intensity at any point along the wavefront will then reduce as the square of the distance traveled by the wave (Gauss' theorem). A factor representing the apparent loss in pressure amplitude due to spherical spreading along an eigenray of length D can be written as

$$L_{SS}(D) = \sqrt{\frac{1}{D^2}} = \frac{1}{D}. \quad (4)$$

When sound propagates in the ocean, part of the acoustic energy is continuously transformed into heat. This absorption is primarily due to the volume viscosity as a result of relaxation processes in seawater. An empirical expression for the attenuation coefficient β (dB/km) at a frequency f (kHz), between 3 and 500 kHz), salinity S (in ‰) and hydrostatic pressure P (kg/cm²) is given by Brekhovskikh and Lysanov, 1991. At a nominal depth of 10 m, the hydrostatic pressure P is approximately 2×10^5 Pa (i.e., 2 kg/cm²). Based on the attenuation coefficient, a loss factor (in pressure amplitude) can be computed to account for the absorption at distance D along an eigenray. We have

$$\begin{aligned} L_A(D) &= 10^{-[(D/1000)\beta]/20} = \exp\left[-\frac{D}{20\,000}\beta \log_e 10\right] \\ &= \exp\left[-\frac{\log_e 10}{20\,000} D 8669 \left(\frac{SAf_T f^2}{f_T^2 + f^2} + \frac{Bf^2}{f_T}\right)\right] \\ &= \exp\left[-0.998D \left(\frac{SAf_T f^2}{f_T^2 + f^2} + \frac{Bf^2}{f_T}\right)\right]. \end{aligned} \quad (5)$$

The attenuation coefficient does not change significantly with small changes in depth. As the depth is constrained in a very shallow water channel, we may use this expression in WSWA channels without a significant loss in accuracy.

The impedance mismatch between the seawater and air causes the sea surface to be a very good reflector. If the sea surface is calm, the reflection is close to perfect but includes a phase shift by π radians, i.e., the reflection coefficient is -1 (Brekhovskikh and Lysanov, 1991). If the sea surface is rough (due to waves), a small loss will be incurred for every surface interaction. We model this loss by allowing a constant loss factor of L_{SR} per surface interaction.

The impedance mismatch between the seawater and seabed causes the sea bottom to reflect some of the sound incident on it. Let ρ and c be the density and sound speed in seawater respectively. Let ρ_1 and c_1 be the density and sound speed in the seabed, respectively. For a smooth sea bottom, the reflection is angle dependent and is given by the Rayleigh reflection coefficient as (Brekhovskikh and Lysanov, 1991)

$$L_B(\theta) = \left| \frac{m \cos \theta - \sqrt{n^2 - \sin^2 \theta}}{m \cos \theta + \sqrt{n^2 - \sin^2 \theta}} \right|, \quad (6)$$

where

$$m = \frac{\rho_1}{\rho}, \quad n = \frac{c}{c_1}.$$

The angle of incidence θ can be computed based on the geometry of the Pekeris waveguide. Let angle θ_{sb} correspond to an eigenray D_{sb} and angle θ_{sb} correspond to an eigenray \underline{D}_{sb} . Then, we have

$$\theta_{sb} = \tan^{-1} \left(\frac{R}{2bh + d_1 - (-1)^{s-b} d_2} \right),$$

$$\theta_{sb} = \tan^{-1} \left(\frac{R}{2bh - d_1 + (-1)^{b-s} d_2} \right). \quad (7)$$

For a rough or absorbing sea bottom, additional reflection losses may be incurred. We model these losses by allowing an additional constant loss factor of L_{BR} per bottom interaction.

B. Time-varying statistical effects

The physics based model described above yields a time-invariant model of the channel. However, the WSWA channel is a time-varying channel. To model the time variation, we introduce some statistical variations in the propagation model.

In line with our initial experimental findings (Chitre et al., 2004), we model the eigenray amplitude as a Rayleigh random process with a median determined by the physics based model and a time-correlation determined by the Doppler spread W_d . Rayleigh fading usually occurs in a sum of a large number of multipath. Rayleigh fading observed on each individual eigenray is thought to occur due to multipath as the eigenray is scattered by small inhomogeneities in the medium and other suspended scatterers (Dashen et al., 1979). This leads to a statistical tapped delay line model which is a special case of the model proposed in Geng and Zielinski (1995), where the tap variation is modeled using Ricean statistics.

The arrival time lag of each eigenray with respect to the direct arrival is related to the difference in path length along the eigenray and the direct path. However, the arrival time lag exhibits variation over time, probably due to movement of the source, receiver and the surface. The stability of the arrival time lag with respect to small changes in source/receiver position can be analyzed using the ray model. Let τ_{sb} be the arrival time lag of eigenray D_{sb} and $\underline{\tau}_{sb}$ be the arrival time lag of eigenray \underline{D}_{sb} . We have

$$\tau_{sb} = \frac{D_{sb} - D_{00}}{c},$$

$$\underline{\tau}_{sb} = \frac{\underline{D}_{sb} - D_{00}}{c}. \quad (8)$$

From Eqs. (1)–(3) and (9), we have

$$\tau_{sb} = \frac{1}{c} \left[\sqrt{R^2 + [2bh + d_1 - (-1)^{s-b} d_2]^2} - \sqrt{R^2 + (d_1 - d_2)^2} \right],$$

$$\underline{\tau}_{sb} = \frac{1}{c} \left[\sqrt{R^2 + [2bh - d_1 + (-1)^{b-s} d_2]^2} - \sqrt{R^2 + (d_1 - d_2)^2} \right]. \quad (9)$$

As we are interested in medium range communications in shallow waters, we assume $R \gg d_1$, $R \gg d_2$ and $R \gg h$. Using the Taylor series expansion $\sqrt{1+x} \approx 1 + \frac{1}{2}x$ if $|x| \ll 1$, we have

$$\tau_{sb} = \frac{R}{c} \left[\sqrt{1 + \left[\frac{2bh + d_1 - (-1)^{s-b} d_2}{R} \right]^2} - \sqrt{1 + \left(\frac{d_1 - d_2}{R} \right)^2} \right] \approx \frac{R}{c} \left[1 + \frac{1}{2} \left[\frac{2bh + d_1 - (-1)^{s-b} d_2}{R} \right]^2 - 1 - \frac{1}{2} \left(\frac{d_1 - d_2}{R} \right)^2 \right]$$

$$= \frac{1}{2Rc} [(2bh + d_1 - (-1)^{s-b} d_2)^2 - (d_1 - d_2)^2]$$

$$= \frac{2}{Rc} [b^2 h^2 + bhd_1 - (-1)^{s-b} bhd_2 + (s-b)d_1 d_2]. \quad (10)$$

Similarly,

$$\underline{\tau}_{sb} \approx \frac{2}{Rc} [b^2 h^2 - bhd_1 + (-1)^{b-s} bhd_2 + (b-s)d_1 d_2].$$

To test the stability of arrival time lag, we differentiate the previous equation with respect to the source depth d_1 , receiver depth d_2 and range R to obtain

$$\frac{\partial \tau_{sb}}{\partial R} = \frac{\partial \underline{\tau}_{sb}}{\partial R} \approx 0, \quad (11)$$

i.e., the arrival time jitter is, to first order, independent of the range, and

$$\begin{aligned}\frac{\partial \tau_{sb}}{\partial d_1} &= \frac{2bh}{Rc} + (s-b)\frac{2d_2}{Rc}, \\ \frac{\partial \tau_{sb}}{\partial d_2} &= -(-1)^{s-b}\frac{2bh}{Rc} + (s-b)\frac{2d_1}{Rc}, \\ \frac{\partial \underline{\tau}_{sb}}{\partial d_1} &= -\frac{2bh}{Rc} + (b-s)\frac{2d_2}{Rc}, \\ \frac{\partial \underline{\tau}_{sb}}{\partial d_2} &= (-1)^{b-s}\frac{2bh}{Rc} + (b-s)\frac{2d_1}{Rc}.\end{aligned}\quad (12)$$

Using Δ as a small change operator, we can write the change in arrival time lag as a function of the change of the source depth, receiver depth and range as

$$\begin{aligned}\Delta \tau_{sb} &= \frac{\partial \tau_{sb}}{\partial R} \Delta R + \frac{\partial \tau_{sb}}{\partial d_1} \Delta d_1 + \frac{\partial \tau_{sb}}{\partial d_2} \Delta d_2, \\ \Delta \underline{\tau}_{sb} &= \frac{\partial \underline{\tau}_{sb}}{\partial R} \Delta R + \frac{\partial \underline{\tau}_{sb}}{\partial d_1} \Delta d_1 + \frac{\partial \underline{\tau}_{sb}}{\partial d_2} \Delta d_2.\end{aligned}\quad (13)$$

As the derivatives with respect to R are 0, the arrival time lags are not sensitive to small changes in range. If we model Δd_1 and Δd_2 as Gaussian random variables with variance σ_d^2 , we can estimate the variance of the arrival time lags as

$$\begin{aligned}\sigma_{\tau_{sb}}^2 &= \sigma^2(\tau_{sb}) = \left| \frac{\partial \tau_{sb}}{\partial d_1} \right|^2 \sigma_d^2 + \left| \frac{\partial \tau_{sb}}{\partial d_2} \right|^2 \sigma_d^2 = \frac{4\sigma_d^2}{R^2 c^2} [2b^2 h^2 \\ &+ (s-b)(d_1^2 + d_2^2 + 2bhd_1 + 2bhd_2)].\end{aligned}\quad (14)$$

Similarly,

$$\begin{aligned}\sigma_{\underline{\tau}_{sb}}^2 &= \sigma^2(\underline{\tau}_{sb}) = \frac{4\sigma_d^2}{R^2 c^2} [2b^2 h^2 + (b-s)(d_1^2 + d_2^2 - 2bhd_1 \\ &- 2bhd_2)].\end{aligned}$$

From this expression, we expect that we have less arrival time lag jitter at further ranges than nearer ranges. We also expect that the arrival time lag jitter increases as the number of surface and bottom interactions of the eigenray increases.

C. The channel model

In the previous two sections, we have developed the components of a time-varying channel propagation model. We now put the components together. Let $x(t)$ be a signal transmitted through the channel and $y(t)$ be the corresponding received signal. Ignoring the absolute time delay between transmission and reception, we can express $y(t)$ in terms of $x(t)$ as

$$\begin{aligned}y(t) &= A_{00}(t)L_{SS}(D_{00})L_A(D_{00})x(t) \\ &+ \sum_{s=1}^{\infty} \sum_{b=s-1}^s A_{sb}(t)L_{SS}(D_{sb})L_A(D_{sb}) \\ &\times (-L_{SR})^s L_{BR}^b L_B(\theta_{sb})^b x(t - \tau_{sb} + J_{sb}(t))\end{aligned}$$

$$\begin{aligned}&+ \sum_{b=1}^{\infty} \sum_{s=b-1}^b A_{sb}(t)L_{SS}(D_{sb})L_A(D_{sb})(\times \\ &- L_{SR})^s L_{BR}^b L_B(\theta_{sb})^b x(t - \underline{\tau}_{sb} + \underline{J}_{sb}(t)) + n(t), \\ \therefore y(t) &= \frac{A_{00}(t)L_A(D_{00})}{D_{00}} x(t) \\ &+ \sum_{s=1}^{\infty} \sum_{b=s-1}^s \frac{A_{sb}(t)L_A(D_{sb})(-L_{SR})^s L_{BR}^b L_B(\theta_{sb})^b}{D_{sb}} x(t \\ &- \tau_{sb} + J_{sb}(t)) \\ &+ \sum_{b=1}^{\infty} \sum_{s=b-1}^b \frac{A_{sb}(t)L_A(D_{sb})(-L_{SR})^s L_{BR}^b L_B(\theta_{sb})^b}{D_{sb}} x(t \\ &- \underline{\tau}_{sb} + \underline{J}_{sb}(t)) + n(t),\end{aligned}\quad (15)$$

where $A_{sb}(t)$ and $\underline{A}_{sb}(t)$ are modeled as independent Rayleigh processes with unit mean and an exponential autocorrelation specified by the Doppler spread W_d . These processes represent the fading of individual eigenpaths. The quantities $J_{sb}(t)$ and $\underline{J}_{sb}(t)$ are random variables denoting the time jitter, modeled as Gaussian processes with zero mean, variance σ_{sb}^2 and an exponential autocorrelation specified by a transducer position coherence time τ_d . The noise $n(t)$ is modeled as a S α S process with characteristic exponent α and dispersion γ (Samorodnitsky and Taqqu, 1994). We assume the noise to be white over the bandwidth of interest. This assumption is reasonable provided the signal bandwidth is not very large.

Although the summations in Eq. (16) have an infinite number of terms, the terms diminish in magnitude and the summations converge. Only terms significantly larger than the ambient noise need to be included in practice. For most channels, it is sufficient to include the first few terms in both summations.

This channel model should be interpreted as a passband channel model. The L_A terms in the model are frequency dependent. If the bandwidth of the signal $x(t)$ is much smaller than the carrier frequency F_c , the L_A terms can be computed at the carrier frequency. For broadband transmission at long distances, this approach yields lower accuracy. However, for simplicity in the analytical model, we use the L_A terms at frequency F_c irrespective of the bandwidth of the signal.

A baseband channel model can also be implemented with some small changes. The L_A terms have to be computed at the appropriate carrier frequency. In addition, the real S α S ambient noise process $n(t)$ needs to be replaced with an isotropic complex S α S noise process (Samorodnitsky and Taqqu, 1994) to accommodate the complex noise requirement at baseband.

This channel model can be interpreted as a tapped delay line with time-varying tap weights and tap delays. Equation (16) can be written in a compact form with N significant terms, appropriate lumped coefficients B_j , delays τ_j , Rayleigh random processes $A_j(t)$, Gaussian random processes $J_j(t)$ and a S α S random process $n(t)$:

$$y(t) = A_0(t)B_0x(t) + \sum_{j=1}^{N-1} A_j(t)B_jx(t - \tau_j + J_j(t)) + n(t). \quad (16)$$

III. EXPERIMENTAL CALIBRATION AND VALIDATION

A. Validation of model against channel measurements

Channel measurements were conducted in February 2004 in Singapore waters to validate the model (Chitre *et al.*, 2004). The chosen location allowed measurements up to 1 km range in a relatively flat area with an average depth of about 15 m. Transmissions were made from an omnidirectional transducer located at the bottom of a 4 m pole mounted on the bow of a research vessel. The signal was received using a hydrophone located at the bottom of a 4 m pole mounted on the side of an anchored barge. The signal was sampled at 250 kSa/s and stored for later analysis. The research vessel moved to various locations and made transmissions. Global positioning system coordinates of the vessel and the barge were noted for range computation. The signal used was a 30 ms direct sequence spread spectrum binary phase-shift keying (BPSK) signal with a bandwidth of 40 kHz centered around 40 kHz. The signal was repeated 100 times at a rate of 10 Hz at each location of the research vessel. The different transmission locations corresponded to ranges of 50, 100, 550, 780, and 1020 m. The measurements were made in relatively calm weather over a period of an hour. The recorded signals were postprocessed using the sign correlator (Chitre *et al.*, 2006) to obtain estimates of the time variability of the multipath structure of the channel. The sign correlator is a near-optimal detector of signals in presence of impulsive snapping shrimp noise. The fading behavior of the signal was determined using the maximum likelihood (ML) estimator (Chitre *et al.*, 2006). The ML estimator is an optimal estimator of signal strength in the presence of snapping shrimp noise with a known probability distribution. The S α S distribution assumed for the ML estimator was calibrated using ambient noise samples recorded at the experimental site.

1. Fading statistics

The fading behavior of the direct arrival at short ranges was determined by estimating the signal strength of 100 μ s sections of the received signal using the ML estimator. Doppler spreads in the range of 5–10 Hz were observed for all ranges. Figure 2 shows the fading of a single path as compared to Rayleigh fading at 50 m range. The observed fading is similar, but slightly less severe than predicted by the Rayleigh distribution. At longer ranges, multiple arrivals are often too closely spaced to separate. At 1020 m, the first arrival is formed by the interference of the direct and surface reflected arrival at this range. Hence one would expect that the fading could be explained as a function of the fading of each of the arrivals. As the time difference between the arrivals is small as compared to the reciprocal of the center frequency of the signal, we may assume that the two arrivals interfere

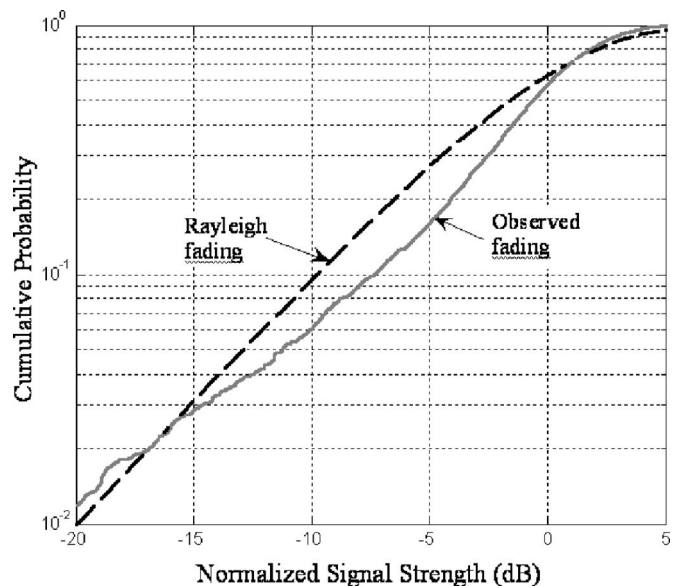


FIG. 2. Cumulative distribution function of signal strength showing fading behavior of direct arrival at 50 m, compared against Rayleigh fading.

destructively as the surface reflection coefficient is -1 . The resulting first arrival would then be distributed as the difference of two independent Rayleigh random variables. Figure 3 shows the fading of the first arrival at 1020 m against simulated fading based on the difference of two Rayleigh random variables. The remarkable similarity in the simulated fading and the observed fading, suggests that the simple model presented earlier is a good approximation.

2. Multipath structure

We compare the measured multipath structure in the channel over 100 transmissions against simulation results. Figure 4 shows a comparison between experiment and simulation in a 15 m deep channel at a range of 100 m. Although

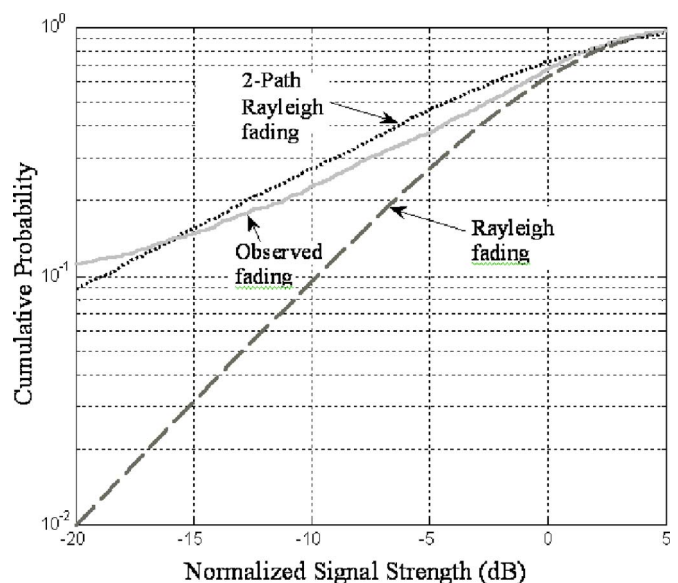


FIG. 3. (Color online) Cumulative distribution function of signal strength showing fading behavior of the combined arrival at 1020 m, compared against Rayleigh fading and simulated two-path Rayleigh fading.

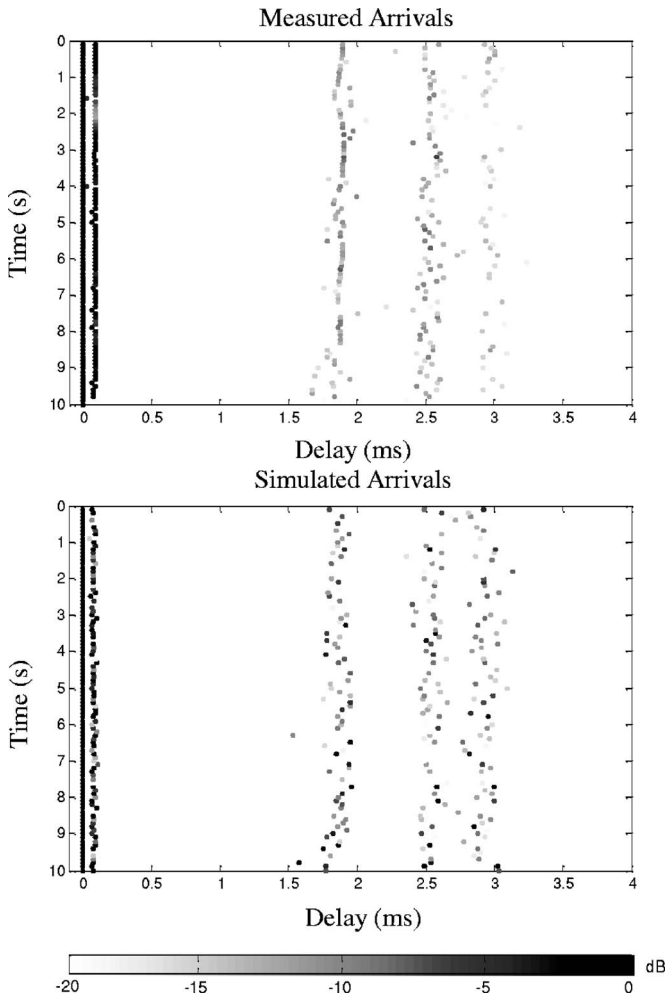


FIG. 4. Comparison of multipath arrival structure between experiment and simulation at 100 m.

similar validations were successfully performed at the longer ranges, we present the results at 100 m due to the high signal-to-noise ratio at this range. This enabled us to study the similarities and differences between the experimental measurements and simulation in more detail than at greater ranges. The simulation parameters were chosen based on our knowledge of the experimental environment. Some channel parameters were tuned slightly to obtain a close match between measurement and simulation. The parameter values used in the simulation are listed in Table I.

Both experimental and simulated arrival structures show five arrivals. The first arrival is the direct arrival, closely followed by the surface reflected arrival and then the bottom reflected arrival. The next three arrivals are a result of multiple surface and bottom interactions. We note that the mean arrival timings (relative to the direct arrival) agree closely between the simulation and measurement, as shown in Table II. The simulation also predicts the spread (standard deviation) of arrival time accurately. The measured data show some correlation between the arrival times of closely spaced iterations for some of the arrivals; this correlation is not captured in our simulation. The correlation is due to the fact that the channel varies slowly over time and hence is correlated over short time intervals. However, this correlation is not important if the transmission time between packets is large.

TABLE I. Parameters used for simulation of channel at 100 m.

Parameter	Symbol	Value
Range ^a	R	100 m
Water depth ^a	h	14.5 m
Source depth ^a	d_1	3 m
Receiver depth ^a	d_2	2 m
Center frequency	F_c	40 kHz
Sampling frequency	F_s	500 kHz
Surface reflection loss ^b	L_{SR}	3 dB
Bottom reflection loss ^b	L_{BR}	10 dB
Water density ^a	ρ	1023 kg/m ³
Water sound speed ^a	c	1539 m/s
Seabed density ^b	ρ_1	1500 kg/m ³
Seabed sound speed ^b	c_1	1650 m/s
Doppler spread ^c	W_d	10 Hz
Ambient noise α^a	α	1.7
Ambient noise level (integrated over the frequency band of interest) ^a	$\gamma^{1/\alpha}$	120 000 μ Pa
Transducer RMS movement ^c	σ_d	0.25 m
Transducer position coherence time ^c	τ_d	0.25 s
Number of reflection terms	N	3

^aThe range, water depth, source, and receiver depths, water density, sound speed and ambient noise parameters were measured at the experiment site.

^bThe surface and bottom reflection losses and the seabed density and sound speed were fitted to the measured data. The values are consistent with known seabed type observed in the area.

^cThe Doppler spread and the transducer rms movement and coherence time were estimated based on the recorded data.

The average measured and predicted arrival strengths (relative to the direct arrival) are quite close. The simulation predicts a little more fading than observed in the direct and surface reflected arrival. It also predicts a few stronger arrivals than those observed in the bottom reflected ray and higher order reflected rays. The slight mismatch in fading statistics between observation and simulation is a limitation of our model as we modeled all arrivals with similar fading statistics. Although a more comprehensive fading model could have been developed, we opted to retain our simple fading model, as the proposed channel model seems to capture most of observed phenomenon in the channel. As we shall see in the next section, communication performance predictions based on this model agree closely with experiment.

TABLE II. Comparison of simulated channel statistics against experimental channel statistics at 100 m.

Arrival		Simulation	Measurement
2	Mean arrival timing (ms)	0.08	0.09
	Arrival timing spread (ms)	0.01	0.01
	Mean relative strength (dB)	0	1
3	Mean arrival timing (ms)	1.9	1.9
	Arrival timing spread (ms)	0.08	0.07
	Mean relative strength (dB)	-7	-8
4	Mean arrival timing (ms)	2.5	2.5
	Arrival timing spread (ms)	0.07	0.07
	Mean relative strength (dB)	-9	-9
5	Mean arrival timing (ms)	2.9	3.0
	Arrival timing spread (ms)	0.07	0.09
	Mean relative strength (dB)	-9	-11

TABLE III. Predicted and actual performance results of OFDM communication schemes at various ranges.

Number of carriers	Cyclic prefix		Communication range	Simulated BER	Experimentally measured BER
	length	Code			
128	32	None	800 m	8.1×10^{-2}	8.0×10^{-2}
128	32	1/3	800 m	0.8×10^{-3}	0.7×10^{-3}
128	32	1/6	800 m	$<10^{-4}$	$<10^{-4}$
512	32	None	800 m	1.2×10^{-1}	1.2×10^{-1}
512	32	1/6	800 m	$<10^{-4}$	$<10^{-4}$
128	32	None	1 km	0.8×10^{-1}	1.0×10^{-1}
128	32	1/3	1 km	1.0×10^{-3}	1.5×10^{-3}
128	32	1/6	1 km	$<10^{-4}$	$<10^{-4}$
512	32	None	1 km	1.1×10^{-1}	1.0×10^{-1}
512	32	1/3	1 km	6.1×10^{-3}	6.0×10^{-3}
512	32	1/6	1 km	$<10^{-4}$	$<10^{-4}$

B. Validation of communications simulation against experimental results

Comparing simulated communication results against experimental results further validates the channel model. The communication scheme chosen was an interleaved coded orthogonal frequency-division multiplexing (OFDM) scheme as described in Chitre *et al.* (2005). The OFDM carriers were modulated using differential quadrature phase-shift keying (QPSK) and occupied a 24 kHz band centered at 62 kHz. Various combinations of the number of carriers, cyclic prefix length, and code rates were tested. Randomly generated data packets were coded using a convolution code or a serial concatenated convolution code. These data were interleaved and modulated using the chosen OFDM scheme and transmitted through the channel. At the other end, it was demodulated, deinterleaved and decoded using a 1-norm Viterbi decoder (Chitre *et al.*, 2007). By comparing the generated data against the decoded data, the bit error rate (BER) was estimated. Various transmission ranges were tested in simulation and in experiment.

The results are shown in Table III. The experimentally measured BER values closely agree with the BER predictions based on simulation using the channel model developed in this paper. Similar measurements with other communication schemes and channel parameters such as number of carriers (64, 128, 256, 512), prefix length (32, 64), code rate (1, 1/2, 1/3, 1/5, 1/6), and transmission range (500 m, 800 m, 1 km, 1.2 km) showed that the predictions were robust to such changes.

IV. CONCLUSIONS

The primary aim of the channel model developed in this article is to enable the study of communication systems in warm shallow waters. The close agreement obtained between the simulated and experimental communication in warm shallow water channels suggests that our model captures the essential physics of such channels. The model captures the multipath arrival structure and includes statistical effects in the channel such as fading and arrival-time jitter. The model predicts the multipath arrival structure, fading probability distribution and arrival-time probability distribution given

the channel geometry. However, the time correlation of the fading is defined by the Doppler spread, which is an input to the model. The Doppler spread has to be measured to calibrate the model and cannot be predicted by the model. The time correlation of the arrival-time jitter is not modeled. This does not affect short transmissions where the arrival-time does not vary over the length of the data packet. However, we expect that this may affect simulations where the data packet length is much larger than the coherence time of the arrival-time jitter.

ACKNOWLEDGMENTS

The author would like to acknowledge the Defence Science & Technology Agency (DSTA), Singapore, for their funding support for this research. He would also like to thank Mr. Shiraz Shahabudeen, Mr. Alan Low, Mr. Koay Teong Beng and Dr. Paul Seekings who helped collect the experimental data used for the validation of the model.

- Badiey, M., Mu, Y., Simmen, J. A., and Forsythe, S. E. (2000). "Signal variability in shallow-water sound channels," *IEEE J. Ocean. Eng.* **25**, 492–500.
- Brekhovskikh, L. M., and Lysanov, Y. (1991). *Fundamentals of Ocean Acoustics*, 2nd ed. (Springer, Berlin).
- Catipovic, J. A. (1990). "Performance limitations in underwater acoustic telemetry," *IEEE J. Ocean. Eng.* **15**, 205–216.
- Chitre, M. (2006). "Underwater acoustic communications in warm shallow water channels," *Faculty of Engineering* (National University of Singapore, Singapore).
- Chitre, M., Ong, S. H., and Potter, J. (2005). "Performance of coded OFDM in very shallow water channels and snapping shrimp noise," *IEEE Oceans'05*, Washington, DC.
- Chitre, M., Potter, J., and Ong, S. H. (2004). "Underwater acoustic channel characterisation for medium-range shallow water communications," *IEEE Oceans 2004*, Kobe, Japan, pp. 40–45.
- Chitre, M. A., Potter, J. R., and Ong, S. H. (2006). "Optimal and near-optimal signal detection in snapping shrimp dominated ambient noise," *IEEE J. Ocean. Eng.* **31**(2), 497–503.
- Chitre, M. A., Potter, J. R., and Ong, S. H. (2007). "Viterbi decoding of convolutional codes in symmetric α -stable noise," *IEEE Trans. Commun.* (in press).
- Coates, R. F. W. (1989). *Underwater acoustic systems* (Wiley, New York).
- Dashen, R., Munk, W. H., Watson, K. M., Zachariasen, F., and Flatte, S. M. (1979). *Sound Transmission through a Fluctuating Ocean* (Cambridge University Press, Cambridge, UK).
- Essebbar, A., Loubet, G., and Vial, F. (1994). "Underwater acoustic channel simulations for communications," *IEEE Oceans'94*, Brest, France, pp. III/495–III/500.
- Galvin, R., and Coates, R. F. W. (1994). "Analysis of the performance of an underwater acoustic communication system and comparison with stochastic model," *IEEE Oceans'94*, Brest, France, pp. III/478–III/482.
- Geng, X., and Zielinski, A. (1995). "An eigenpath underwater acoustic communication channel model," *IEEE Oceans'95*, San Diego, pp. 1189–1196.
- Owen, R. H., Smith, B. V., and Coates, R. F. W. (1994). "An experimental study of rough surface scattering and its effects on communication coherence," *IEEE Oceans'94*, Brest, France pp. 483–488.
- Potter, J. R., Lim, T. W., and Chitre, M. (1997a). "Ambient noise environments in shallow tropical seas and the implications for acoustic sensing," *Oceanology International 97 Pacific Rim*, Singapore, pp. 191–199.
- Potter, J. R., Lim, T. W., and Chitre, M. (1997b). "High-frequency ambient noise in warm shallow waters," *Sea Surface Sound*, Southampton, UK, pp. 45–54.
- Proakis, J. G. (1995). *Digital Communications* (McGraw-Hill, Singapore).
- Samorodnitsky, G., and Taqqu, M. S. (1994). *Stable Non-Gaussian Random Processes* (Chapman and Hall, New York).
- Stojanovic, M. (1996). "Recent advances in high-speed underwater acoustic communications," *IEEE J. Ocean. Eng.* **21**, 125–136.
- Tsirintzis, G. A., and Nikias, C. L. (1995). "Performance of optimum and suboptimum receivers in the presence of impulsive noise modeled as an alpha-stable process," *IEEE Trans. Commun.* **43**, 904–914.